Determine the Function of a Specific Immunoglobulin Domain of Titin in Zebrafish

BY

XINGHANG JIANG
M.S., Illinois Institute of Technology, 2015
B.S., China Agricultural University, 2013

THESIS

Submitted as partial fulfillment of the requirements
for the degree of Master of Science in Biological Sciences
in the Graduate College of the
University of Illinois at Chicago, 2020

Chicago, Illinois

Defense Committee:

David Stone, Chair
Ankur Saxena, Advisor
Peter Okkema

ACKNOWLEDGMENTS

I would like to express my deep and sincere gratitude to my research advisor, Dr. Ankur Saxena, for his continuous support and guidance in this project and my study. His knowledge, patience, motivation, and frankness helped me make progress in my research and become mature. I also would like to thank my committee (Dr. David Stone, Dr. Ankur Saxena, and Dr. Peter Okkema) for giving me this opportunity to continue my study and helping me in the program.

I thank my lab members in the Saxena lab: Lynne Nacke, Joe Lombardo, Sriivatsan G. Rajan, and Vijay Warrier for their suggestions for this thesis and endless supports and encouragements; Fritz Navales and Karina Oye for their help on genotyping and screening; Katie Harvey for her lovely zebrafish cartoons; Randall Treffy for his “medical” support; Kaelan Wong, Jagjot Dhingra and Nathan Burg for their support to keep my zebrafish alive.

I thank Dr. Dawood Darbar and his lab at the Department of Medicine, UIC, for the wonderful collaboration and continuous support.

I also thank my friends Xinyuan Liu, Xin Wang and Hsiang-Chun Chang for their help during the pandemic and revising my thesis.

Xinghang Jiang

TABLE OF CONTENTS

LIST OF TABLES

LIST OF FIGURES

LIST OF ABBREVIATIONS

AF	Atrial Fibrillation
AS-PCR	Allele-Specific Polymerase Chain Reaction
cmcl2	cardiac myosin light chain 2
CRISPR-Cas9	Clustered Regularly Interspaced Short Palindromic Repeats and CRISPR Associated Protein 9
dpf	days post-fertilization
ECG	Electrocardiography
EDA	End-Diastolic Area
EDV	End-Diastolic Volume
EF	Ejection Fraction
EOAF	Early-Onset Atrial Fibrillation
ESA	End-Systolic Area
ESV	End-Systolic Volume
FAC	Factional Area Change
HDR	Homology-Directed Repair
Ig	Immunoglobulin
NHEJ	Non-Homologous End Joining
ssODN	single-strand oligonucleotide
SV	Stroke Volume

SUMMARY

Mutations in genes encoding cardiac ion channels, transcription factors, and myocardial structural proteins have been identified in patients with early-onset atrial fibrillation (EOAF). However, the underlying mechanisms by which structural proteins give rise to atrial fibrillation (AF) remain unclear. Titin (*TTN*) is a multi-domain protein essential for sarcomere assembly during heart development and the restoration of normal sarcomere length after cardiomyocyte contraction. Previous work on a truncated *TTN* suggested that disruption of the sarcomeric organization may lead to EOAF. However, it remains unknown what role a specific *TTN* domain might play in abnormal sarcomere development and/or maturation. Our collaborator identified a *TTN* missense mutation (T31115I) in a patient with EOAF and showed that it co-segregates in the patient's family for three generations. To elucidate whether the T31115I mutant causes AF and what the underlying mechanisms might be, I adopted two CRISPR-Cas9-mediated approaches: 1) homology-directed repair to introduce this mutation into the zebrafish ortholog, *ttna*; and 2) generation of two mutant *ttna* alleles, *ttna*$^{\Delta 6}$ and *ttna*$^{\Delta 9}$, with 6 or 9 amino acids deleted, respectively, within a highly conserved region containing the site of T31115I mutation. *ttna*$^{\Delta 9/\Delta 9}$ zebrafish embryos demonstrated inflow tract edema, pericardial edema, blood clots, atrial enlargement, and reduced cardiac function, as indicated by lower ventricular contraction and cardiac output. These data suggest that the specific region deleted in *ttna*$^{\Delta 9}$ is important for proper cardiac function. As the highly conserved region contains

the EOAF-associated *TTN* point mutation, further investigation of this region may not only reveal more biological pathways that involve titin, but also provide more insights into the pathogenesis of EOAF.

I. INTRODUCTION

A. Atrial fibrillation is the most common arrhythmia.

Over 2.7 million Americans live with atrial fibrillation (AF) (Morillo et al., 2017). During AF episodes, the atrium beats irregularly and is unable to coordinate with the ventricle. AF symptoms often include heart palpitations, dizziness, shortness of breath, and anxiety. It can increase the risk of cardiovascular and cerebrovascular complications, such as heart failure and stroke (Kotecha & Piccini, 2015). Familial early-onset atrial fibrillation (EOAF) is an inherited type of AF with disease onset in a patient younger than 60 years old (Alzahrani et al., 2018). Familial EOAF often results from rare single-gene mutations. Mutations in genes encoding ion channels, such as *KCNQ1*, *KCNA5*, *KCNJ3,* and *KCNJ5* (Bartos et al., 2013; Yamada et al., 2019; Yang et al., 2009), and sarcomeric structural protein coding genes, such as myosin light chain 4 (*MYL4)* and myosin heavy chain 6 (*MYH6)* (Gudbjartsson et al., 2017; Holm et al., 2011; Orr et al., 2016), have been implicated in familiar EOAF. However, the role of other sarcomeric structural proteins in EOAF remains unknown.

B. Titin is a main component in the sarcomere structure.

The intracellular contractile apparatus in cardiomyocytes is organized in cable-like structures called myofibrils. The basic unit in myofibrils that provides the force for muscle cell contraction is called a sarcomere. It is defined as the segment between two neighboring Z-disks, the anchor points for actin filaments (Fig. **1**). The lighter region

around the Z-disk is called the I-band and is mainly composed of actin filaments. The darker region next to the I-band is the A-band and is mainly composed of myosin. M-line is in the center of the A-band and is formed by cytoskeleton cross-linkage (Wang et al., 2018).

Titin, a main sarcomeric protein, is by far the largest protein that has been discovered in the human body. It spans half-length of one sarcomere: from the Z-disk to the M-line. Similar to the sarcomere, titin can also be divided into the I-band and the A-band, which bind to actin filaments and myosin, respectively (Fig. **1**). These interactions are essential for sarcomere assembly (Linke & Hamdani, 2014).

Titin is involved in both the contraction and the relaxation of cardiomyocytes (Fig. **1**). During muscle contraction, titin is required for keeping myosin centered in the sarcomere to optimize the force generated by the relative movement between myosin and actin filaments. During relaxation, titin acts as a molecular spring to provide a negative force. Using this negative force, the I-band generates a passive tension which returns the sarcomere to its noncontractile length (Granzier & Labeit, 2002). Additionally, titin is also involved in mechano-chemical signaling events via some of its binding partners (Linke & Hamdani, 2014).

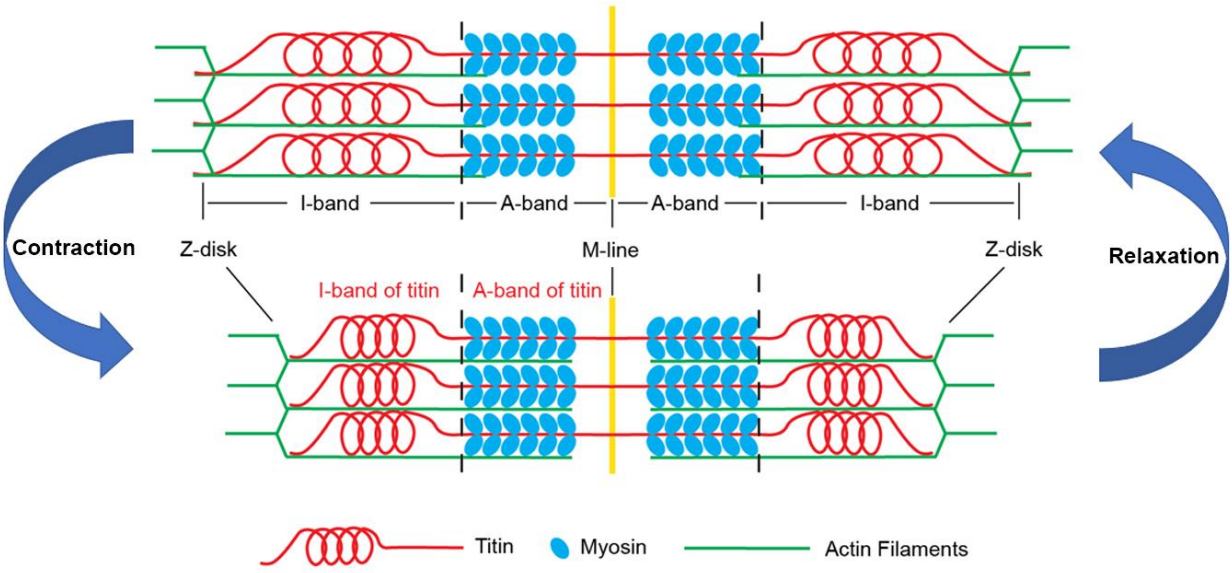

FIGURE 1. Schematic of the sarcomere and its components during contraction and relaxation. Sarcomeres consist of Z-disk, I-band, A-band and M-line. Similarly, titin also is divided into I-band and A-band, indicated in red letters. Red, titin; blue, myosin; green, actin filaments.

C. *TTN* is a major human disease gene and p.T31115I is associated with early-onset atrial fibrillation.

Titin is encoded by *TTN* and expressed in skeletal muscle and both atrial and ventricular cardiomyocytes., *TTN* has been revealed as a major human disease. At least 125 *TTN* mutations have been identified associated with skeletal muscle or heart diseases (Linke & Hamdani, 2014). For example, *TTN* nonsense mutations are identified in approximately 25% of cases of familial dilated cardiomyopathy, and they are the most common genetic causes for this disease (Herman et al., 2012). There are multiple titin isoforms generated from alternative splicing, and they have different degrees of elasticity. The ratio of compliant to stiffer isoforms results in different elasticity of cardiomyocytes (Cazorla et al., 2000). Mutations inducing changes in this ratio may contribute to the altered diastolic passive stiffness in heart diseases (Linke & Hamdani, 2014). Nonsense mutations (Ahlberg et al., 2018) and loss-of-function mutations (Choi et al., 2018) of *TTN* are associated with EOAF. In our model system, zebrafish, the disorganized sarcomere has been proposed as a potential mechanism for these associations (Ahlberg et al., 2018).

Our collaborator Dr. Dawood Darbar (Department of Medicine, University of Illinois at Chicago (UIC)), found a missense mutation in *TTN* in an EOAF patient enrolled in the UIC AF Registry. The mutation locates at chr2:178539798, in which the guanine is mutated to adenine, resulting in a threonine (T) substitution to isoleucine (I) in amino acid 31115 based on UniProt Q8WZ42. This point mutation was identified by performing whole

exome sequencing and bioinformatics filtering based on rarity, ethnicity, co-segregation with AF, predicted pathogenicity, and internal reference exomes. The amino acid substitution induced by this mutation is in the immunoglobulin (Ig) domain 139 (Ig-139), one of 166 Ig domains in titin protein. Forty-five Ig domains form with Fibronectin type-III (FN3) domains into two super-repeats regions, D-zone and C-zone, in the A-band of titin (Linke & Hamdani, 2014). Ig-139 is the last Ig domain of the last repeat in the C-zone (Fig. **2A, B**).

D. <u>Zebrafish as a model organism for cardiac research</u>

The zebrafish (*Danio rerio*) has become a popular model organism because of its ability to produce a large number of progeny and its ease of genetic manipulation. Additionally, its rapid development allows for many developmental processes to be observed in a relatively short period of time (Letrado et al., 2018). It shares 71.4% of genes in common with humans (Howe et al., 2013), and about 82% of human disease-associated genes have a zebrafish ortholog (Lam & Peterson, 2019).

The zebrafish is an attractive model organism particularly for cardiac research. Its embryonic optical transparency and ventrally positioned heart allow the use of high-resolution live imaging to assess cardiac development and function. Around 24 hours post-fertilization (hpf), a cardiac disk formed by mesodermal cells elongates to form a linear heart tube and starts contracting. By 48 hpf, it loops leftward and forms a two-chambered heart. During larval and early juvenile stages, the heart rotates such that the

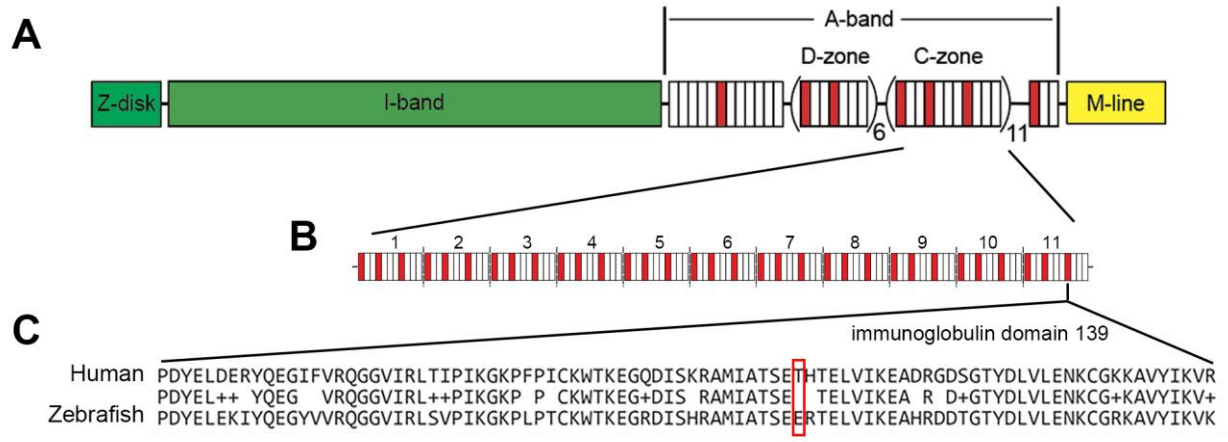

FIGURE 2. The early-onset atrial fibrillation associated *TTN* point mutation is in the immunoglobulin domain 139 of titin A-band. (A) Schematic of the full-length human titin protein. **(B)** Detailed layout of the C-zone in A-band. Red, immunoglobulin (Ig) domain. White, Fibronectin type-III (FN3) domain. There are 11 repeats of Ig-FN3-FN3-Ig-FN3-FN3-FN3-Ig-FN3-FN3-FN3 pattern of domains in the C-zone. **(C)** Amino acid sequence alignment of immunoglobulin domain 139 (Ig-139) of human titin protein and its corresponding Ig domain in the zebrafish ttna protein. The red box indicates the location of residue affected by the EOAF-associated *TTN* point mutation.

ventricle is positioned ventrally to the atrium (Brown et al., 2016). The two-chamber heart of zebrafish provides a simplified model to work with, and some of its unique features make the zebrafish a superior organism to study certain cardiovascular diseases. The zebrafish has a more similar electrophysiology to humans than mice do (Wilkinson et al., 2014). For example, zebrafish and humans have similar durations of atrial and ventricular depolarization and comparable time that the electrical impulse takes to pass from the sinus node through the atrioventricular node (Orr et al., 2016). These similarities of cardiac electrophysiology contribute to similar heart rates. The human heart rate is 60–100 beats per minute (bpm) and that of zebrafish is 120–180 bpm, while that of mice is 300–600 bpm (Poon & Brand, 2013). Additionally, zebrafish can survive up to 7 days post-fertilization (dpf) without a functional cardiovascular system, which facilitates investigating severe cardiac defects in embryos (Sarmah & Marrs, 2016).

There are two *TTN* orthologs in the zebrafish: *ttna* and *ttnb*. The primary ortholog expressed in the heart is *ttna*. It expresses before *ttnb* and plays a more important role in sarcomere assembly and cardiac contractility (Seeley et al., 2007). The amino acid sequence of one ttna Ig domain shares the highest overall homology (80% identity) with the human titin Ig-139 domain. Particularly, within the human Ig-139 domain and corresponding zebrafish Ig domain, the nearby region flanking the EOAF-associated *TTN* point mutation is highly conserved between human and zebrafish (Fig. **2C**).

E. Use CRISPR-Cas9 to generate mutant zebrafish lines

Clustered regularly interspaced short palindromic repeats and CRISPR associated protein 9 (CRISPR-Cas9) has been used as an efficient method to manipulate gene expression transiently, generate stable mutants, and insert endogenous markers. The method uses a single guide RNA (sgRNA) to direct Cas9 protein to generate a double-strand DNA break in the targeted region. The double-strand break will be repaired through either the homology-directed repair (HDR) pathway or the non-homologous end joining (NHEJ) pathway. To knock-in the desired mutation through the HDR pathway, a double or single-strand oligonucleotide (ssODN) can be used as a template. Although using CRISPR-Cas9 to knock-out genes by introducing a premature stop codon or frameshift is very efficient and convenient, knocking-in a specific mutation to introduce a single amino acid substitution is still relatively challenging. That is because compared to NHEJ, HDR is a rare event to repair the DNA break, and NHEJ generates unpredictable insertions or deletions (Banan, 2020).

In this study, I optimized established CRISPR-Cas9 protocols (Bai et al., 2020; Prykhozhij et al., 2018) to increase *TTN*-specific knock-in efficiency in order to 1) introduce the EOAF-associated point mutation into the zebrafish; 2) generate two zebrafish lines with region-specific deletions, with the overarching goal of studying the function of the highly conserved region around the site of EOAF-associated point mutation.

F. Statement and significance of the problem

Even though associations and mechanisms of genes involved in ion channel and cell signaling in EOAF have been widely studied, there are still likely many rare mutations contributing to AF that have not yet been identified because the recently found associations between sarcomeric structural proteins and EOAF provided a new aspect to study the underlying biological pathways that are important for the AF pathogenesis (Ahlberg et al., 2018; Gudbjartsson et al., 2017; Orr et al., 2016). Hence, the understanding of AF pathogenesis is incomplete.

TTN is a major human disease gene (LeWinter & Granzier, 2013). Disease-associated nonsense mutations of *TTN* have been introduced into the zebrafish model to study the pathogenesis of some cardiac diseases, such as AF and dilated cardiomyopathy (Ahlberg et al., 2018; Huttner et al., 2018). However, an EOAF-associated *TTN* missense point mutation in an animal model has not been created. In this study, I'm using CRISPR-Cas9 to knock-in an EOAF-associated *TTN* missense point mutation, found by our collaborator, into the zebrafish to test whether human AF-related phenotypes can be recapitulated in the zebrafish model and to determine the mechanisms underlying EOAF pathogenesis.

The surrounding region of the EOAF-associated *TTN* missense point mutation is highly conserved between human and zebrafish, so I hypothesize that this region has a role in the cardiac function and/or development. To test this hypothesis, I generated two

ttna mutant alleles, *ttna*$^{\Delta 6}$ and *ttna*$^{\Delta 9}$, which deleted several amino acids around the mutation site within this region, and examined zebrafish embryos carrying *ttna*$^{\Delta 6}$ and *ttna*$^{\Delta 9}$ to determine whether these zebrafish exhibit defects in cardiac function and development, including AF-related phenotypes.

G. Purpose of the study

The purpose of this study is 1) to establish a zebrafish model carrying the human EOAF-associated *TTN* missense point mutation to investigate the pathogenesis of EOAF, and 2) to determine the function of the highly conserved region around the point mutation. Investigation of this region may also reveal biological pathways that underlie the pathogenesis of EOAF.

II. METHODS

A. Zebrafish husbandry

Zebrafish were treated and cared for according to the National Institutes of Health Guide for the Care and Use of Laboratory animals. All experiments were approved by the University of Illinois at Chicago Institutional Animal Care Committee. Zebrafish embryos were grown, staged, and collected as previously described (Kimmel et al., 1995; Westerfield, 2000). The transgenic line used was *Tg(cmlc2:eGFP;Gata1:dsRed)* (Zebrafish strain: AB wild-type background)(Huang et al., 2003; Zhu & Zon, 2004).

B. Generation of mutant zebrafish lines

The crRNA was designed to direct the Cas9 protein to the desired location of *ttna* with the online bioinformatics tool, CHOPCHOP. The HDR templates for knocking-in the desired EOAF-associated *TTN* point mutation were designed with the CRISPR function of Benchling, an online informatics platform. Asymmetric HDR template 1 and 2 are single-strand oligonucleotides (ssODN) targeting either the PAM-containing strand or non-PAM strand of genomic DNA with asymmetric homology arms. The long symmetric HDR template is a ssODN targeting the non-PAM strand with long symmetric homology arms. All templates contain silence mutations to prevent repeated cutting of Cas9 protein and create a restriction enzyme digestion site for further screening. The tracrRNA, customized crRNA, Cas9 proteins and HDR templates were ordered from Integrated DNA Technologies (IDT). The injection solution containing assembled ribonucleoproteins and

one of three HDR templates (0.4-1 μM for templates 1 and 2; 42.8 ng/μL for template 3) was prepared according to an established protocol provided by IDT (Essner). The solution was injected (0.7-1.5 nL) into the wild-type AB strain zebrafish embryos at the one-cell stage.

C. Genotyping and sequencing

Genomic DNA of 1-4 dpf zebrafish embryos or tail-clip of adults were extracted with Hot Sodium Hydroxide and Tris (HotSHOT) method: a single embryo, 30 pooled embryos or 3 mm tail-clip were dissolved in 50 mM NaOH and 95°C for 15 min, cooled down and neutralized with 1/10 NaOH volume of 1 M Tris-HCl pH8.0. Allele-specific PCR (AS-PCR) was designed according to a previously described method (Prykhozhij et al., 2018). AS-PCR and genotyping were performed with DreamTaq Hot Start Green PCR Master Mix (Thermo Scientific, K9022). The electrophoresis of PCR products was performed with 1% or 4% agarose gel and imaged with a gel imager (Alpha Innotech). LA Taq DNA polymerase (TaKaRa, RR042B) was used to amplify DNA fragments for regular Sanger sequencing and amplicon next-generation sequencing (NGS) that performed by the Genome Research Core of UIC. Analysis of amplicon NGS was performed with CRISPResso5 (Pinello et al., 2016). All primers were ordered from IDT.

D. Live imaging

To minimize the off-target effect of CRISPR-Cas9, F_0 generation has been outcrossed for two generations, and the F_3 generation was used to perform live imaging

and cardiac function assessments. They were acquired from the incrossing of cmlc2:eGFP; Gata1:dsRed-dual positive heterozygous mutant F_2 generation and tested before I knew their genotypes. During imaging, 2 dpf zebrafish embryos were kept freely in E3 medium, and 4 dpf embryos were embedded in 0.9% low-melting agarose. Lateral view videos of the whole embryo were recorded with Axiocam 506 mono camera (ZEISS) through Axio Zoom.V16 microscope (ZEISS) in brightfield, GFP and RFP channel. Videos were recorded in about 28 frames per second for 350-450 frames at room temperature.

E. Cardiac parameter measurements

The assessments of edema phenotypes were performed using videos in brightfield, and the measurements of heart rhythm and cardiac parameters were performed using videos in GFP channel and cmcl2:eGFP-positive zebrafish as previously described (Yalcin et al., 2017). The heart rhythm was measured and analyzed based on an established method, ZebraPace (Gaur et al., 2018). For cardiac parameters, ImageJ was used to measure the following parameters: area of atria and ventricles at the end-diastolic phase (EDA) and end-systolic phase (ESA), ventricular long diameters (D_L) and short diameters (D_S) at end-diastolic phase and end-systolic phase. The fractional area change (FAC), end-diastolic volume (EDV) and end-systolic volume (ESV) of ventricles, stroke volume (SV) and ejection fraction (EF) were calculated by the following equations:

$$\text{FAC}\ (\%) = \frac{EDA - ESA}{EDA} \times 100$$

$$\text{Volume} = \frac{1}{6} \times \pi \times D_L \times D_S^2$$

$$\mathrm{SV} = \mathrm{EDV} - \mathrm{ESV}$$

$$\mathrm{EF}\ (\%) = \frac{EDV - ESV}{EDV} \times 100$$

F. Statistical analysis

The significance of differences between groups of zebrafish was calculated with unpaired t-tests, and the data in the figure are expressed with mean and 95% confidence interval. Statistical analyses were performed in GraphPad Prism 8 (La Jolla, CA). Data were combined from three independent replications.

TABLE I. Sequences of Guide RNA, HDR Templates and Primers

items	sequence
Target for guide RNA	AAGCTCAGTACGTTCTTCAC
Asymmetric HDR Template 1	C*A*GTGCCCATCAAAGGCAAACCCTTACCAACAT GCAAGTGGACAAAAGAAGGTCGTGACATTTCTCA CAGAGCTATGATCGCAACAAGTGAAATACGTACTG AGCTTGTAATCAAGGAAGCCCA*T*A
Asymmetric HDR Template 2	C*C*TTCCTTCCACATTTATTTTCCAACACAAGATC GTAGGTACCGGTGTCATCTCTATGGGCTTCCTTG ATTACAAGCTCAGTACGTATTTCACTTGTTGCGAT CATAGCTCTGTGAGAAATGTC*A*C
Long Symmetric HDR Template	GGACCCTCAGGTGGATCTGGGCGACCTATAACTT TTACTTTAATATAGACAGCCTTCCTTCCACATTTATT TTCCAACACAAGATCGTAGGTACCGGTGTCATCT CTATGGGCTTCCTTGATTACAAGCTCAGTACGTA TTTCACTTGTTGCGATCATAGCTCTGTGAGAAATG TCACGACCTTCTTTTGTCCACTTGCATGTTGGTAA GGGTTTGCCTTTGATGGGCACTGATAGCCTGATG ACGCCACCTTGTCTGACAACATAGCCTTCCTGG
AS-PCR Forward Primer	TCTACTCAGTCCAGTTTCAT
AS-PCR Reverse Primer for Wild-type Allele	ATGATTGCAACCAGTGAAGA
AS-PCR Reverse Primer for Mutant Allele	ATGATCGCAACAAGTGAAAT
Sanger Sequencing Forward Primer	TTTCTCTTGCTTGGTCTCCTCC
Sanger Sequencing Reverse Primer	TAGGAGGTTCTGGTGGACCTTG
NGS Amplicon Sequencing Forward Primer	ACACTGACGACATGGTTCTACATAGACAGCCTTC CTTCCACATT
NGS Amplicon Sequencing Reverse Primer	TACGGTAGCAGAGACTTGGTCTACCCTGACTATG AGCTGGAAAA
Genotyping Forward Primer for *ttna*$^{\Delta 9}$	GCCTTCCTTCCACATTTATTTTCCA
Genotyping Reverse Primer for *ttna*$^{\Delta 9}$	CAGGCTATCAGTGCCCATCA

All sequences are in 5’ to 3’ direction.

Asterisks: phosphorothioate linkages

Underlined sequence: adapter sequences for amplicon next-generation sequencing

III. RESULTS

A. Genotyping zebrafish embryos to screen for the *TTN* mutation

Because *ttna* is the primary ortholog of *TTN* in the zebrafish heart (Seeley et al., 2007), I aligned the amino acid sequences of human titin Ig-139 domain and the corresponding Ig-domain of zebrafish ttna protein to locate the substitution induced by the EOAF-associated *TTN* point mutation (Fig. **2C**) and found that the ttna residue corresponding to the substituted residue in human titin is glutamate acid (E) instead of threonine (T) in humans. To mimic the amino acid substitution in human titin, I optimized CRISPR-Cas9-mediated homology-directed repair (HDR) to create an E29821I substitution in the zebrafish ttna protein. (Hereafter, the EOAF-associated *TTN* point mutation will be noted as the ***TTN* point mutation**.) I have designed multiple HDR templates to optimize the efficiency of knocking in the *TTN* point mutation. Following the workflow of generating and screening this mutation (Fig. **3**), F_0 and F_1 generations were used to test the efficiency of knock-in and germline transmission.

According to an established method (Prykhozhij et al., 2018), a ssODN with asymmetric homology arms was used as the HDR template (asymmetric HDR template 1) to knock-in the *TTN* point mutation. To rapidly screen the injected embryos for potential founders carrying this mutation, I designed an allele-specific polymerase chain reaction (AS-PCR) approach. Using the same forward primer and allele-specific reverser primers, this method specifically amplifies wild-type or mutant fragments of the same length, 1.2

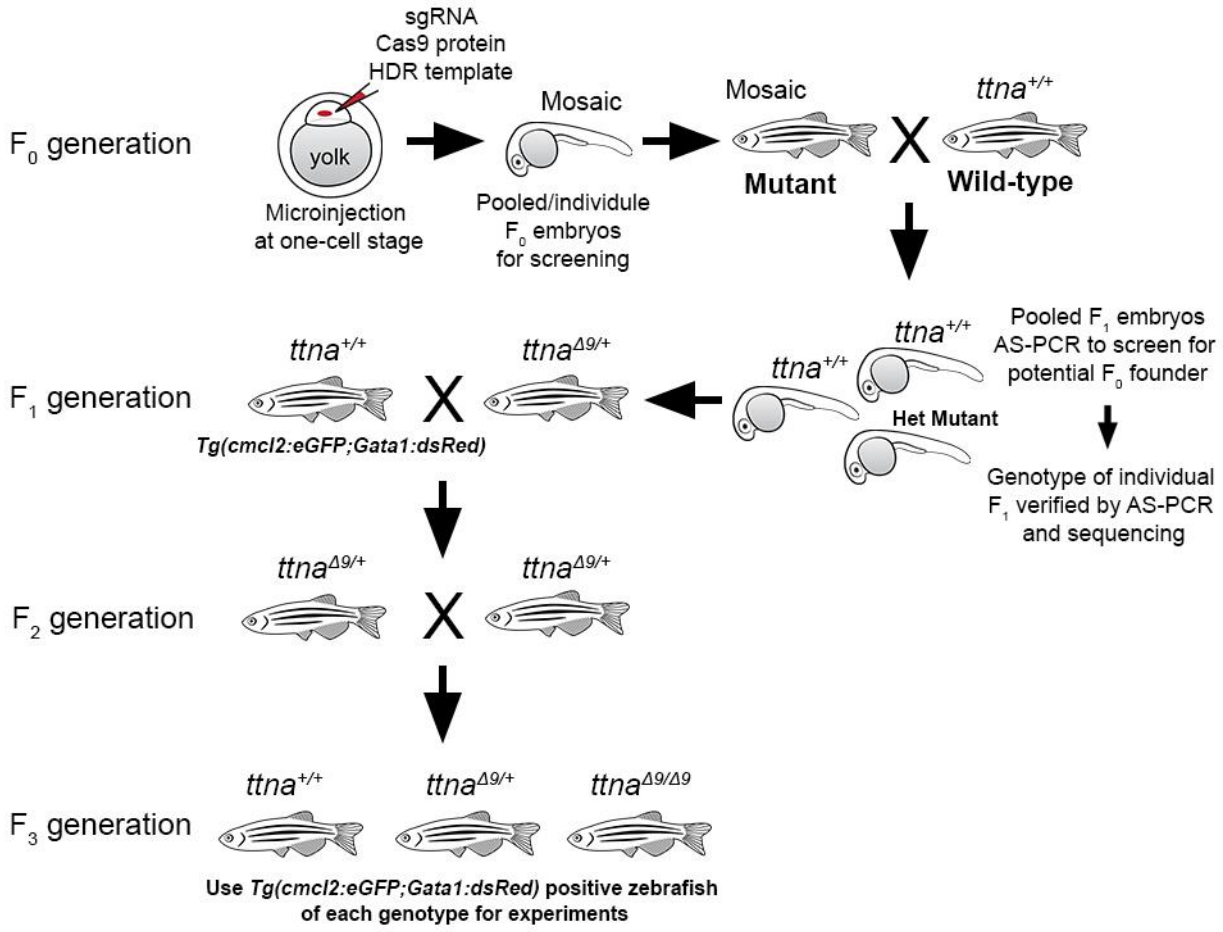

FIGURE 3. **Workflow diagram of generating, screening, and testing mutant zebrafish lines.** Allele-specific PCR (AS-PCR) and amplicon next-generation sequencing (NGS) were performed on injected embryos to test the knock-in efficiency. Actual mutations were confirmed with sequencing on F_1 embryos acquired from injected embryos outcrossing with wild-type zebrafish. The F_1 generation carrying specific *ttna* mutations were outcrossed with a transgenic line to visualize cardiac contraction and red blood cells. The F_3 generation acquired from the F_2 generation incrossing was used to test AF-related phenotypes and cardiac function. The figure shows *ttna*$^{\Delta 9}$ for simplicity.

kb (Fig. **4A**). The AS-PCR results showed the 1.2 kb fragment was amplified by the mutant-specific primers in pooled, injected embryos (F_0) but not in the uninjected control embryos (Fig. **4B**). These data indicate that there were putative correct point mutations in injected embryos and confirm the specificity of AS-PCR to detect the potential correct mutation.

Although the AS-PCR of embryos injected with asymmetric HDR template 1 showed successful amplification of the mutant fragment and next-generation sequencing of the same sample showed 5.4% of the total amplicons carry the correct point mutation (Fig. **4C**), the mutation generated with asymmetric HDR template 1 and 2 has thus far failed to pass to the F_1 generation.

To increase the efficiency of knock-in for improving germline transmission, I switched to a long symmetric HDR template. Embryos injected with 1 nL of injection solution had approximately 10% survival rate at 5 dpf. The single-embryo AS-PCR of these embryos showed more bands that were brighter and smaller than the full-length 1.2 kb band (Fig. **4D**), which indicates that random deletions happened as dominant events. The low survival rate and AS-PCR results also suggest that there might be excessive cutting of Cas9 protein, and a lower amount of Cas9 protein might be needed. Embryos injected with 0.7 nL injection solutions had approximately 50% survival rate at 5 dpf. The single-embryo AS-PCR of 3 out of 4 injected embryos showed a bright 1.2 kb band and a few smaller bands that were dimmer than the 1.2 kb band (Fig. **4D**), which suggests the

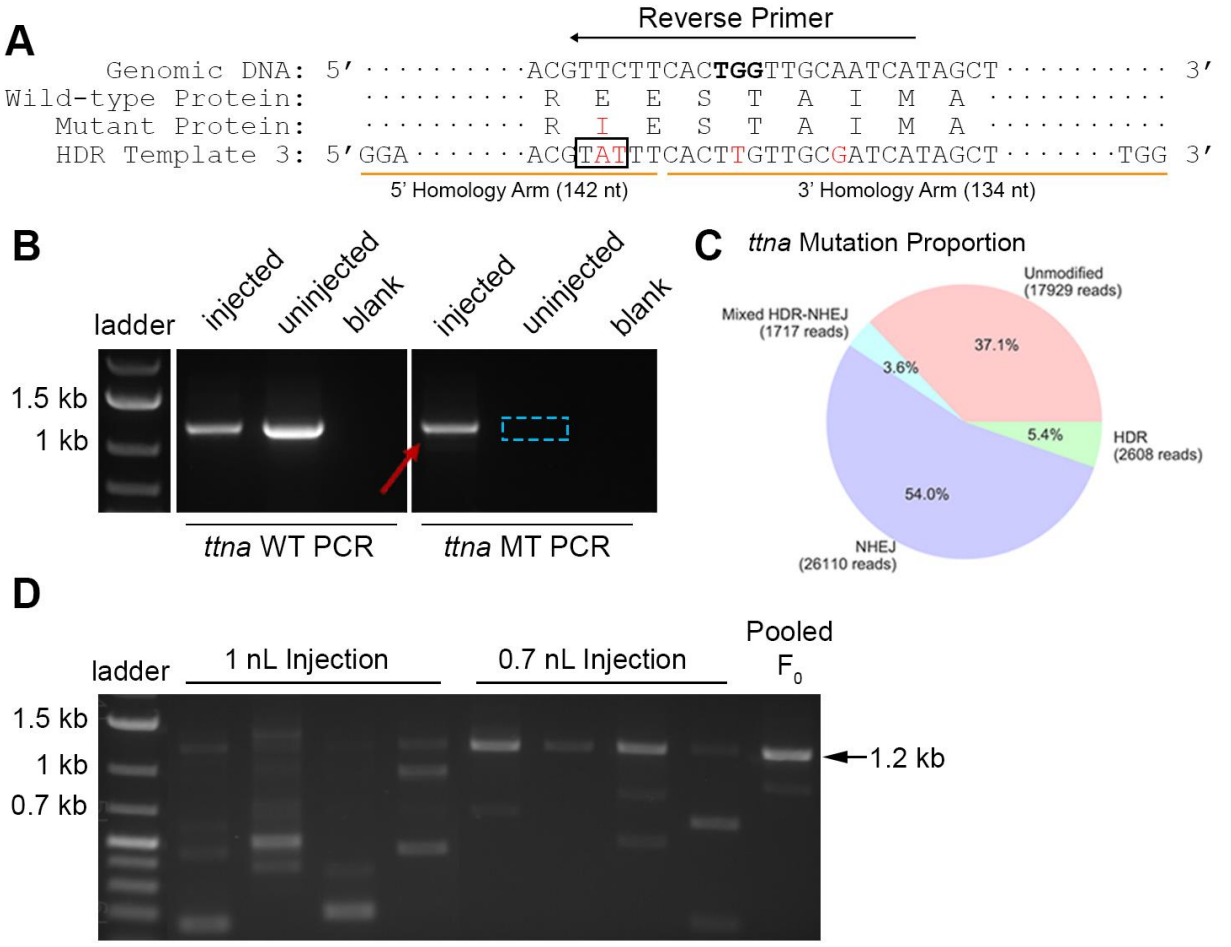

FIGURE 4. Generating and screening for mutant *ttna.* (A) Schematic of CRISPR-Cas9-mediated homology-directed repair (HDR) to introduce the EOAF-associated *TTN* point mutation into the zebrafish ortholog, *ttna*, using long symmetric HDR template. The template was designed to knock-in: the *TTN* point mutation, the silence mutation to prevent repeated cutting of Cas9, and the silence mutation to create a restriction enzyme digestion site for further screening. Reverse primers targeting wild-type or mutant allele in the indicated area are coupled with the same forward primer for AS-PCR to detect the integration of correct mutations. Letters in red, mutations and amino acid substitution introduced; Bolded, protospacer adjacent motif (PAM) site; Boxed, *TTN* mutation site. **(B)** AS-PCR showed the presence of potential mutant allele amplified with in pooled injected F_0 embryos (arrow) and absence in uninjected F_0 embryos (dashed box). PCR products were amplified with wild-type (WT) or mutant (MT) primers; blank = control with primers but no DNA. **(C)** *ttna* HDR knock-in efficiency tested with amplicon NGS and analyzed with CRISPResso5 in pooled injected F_0 embryos. HDR indicates the desired EOAF-associated *TTN* point mutation. NHEJ indicates random mutations near the target site. **(D)** Single-embryo AS-PCR of embryos injected with the long symmetric HDR template and different volumes of injection solution. The pooled F_0 band indicates the 1.2 kb full-length PCR product.

HDR might happen as a dominant event. Even though there was no direct comparison of knock-in efficiency between former asymmetric HDR templates and the long symmetric HDR template, the higher survival rate and the AS-PCR results of the 0.7 nL injection suggest that the long symmetric HDR template and the optimized volume of injection solution may yield a higher efficiency of knocking-in the EOAF-associated *TTN* point mutation to improve germline transmission. The F_1 embryos from potential founders will be genotyped to further test the germline transmission of the optimized method.

B. Two *ttna* mutant zebrafish lines were generated with CRISPR-Cas9.

To better understand the function of the specific region affected by the *TTN* point mutation, I checked the conservation of the nearby region flanking the EOAF-associated missense point mutation site. I found that this region in human titin and zebrafish ttna shares high identity (Fig. **5A**), so I hypothesize that this highly conserved region has a function in cardiac development and/or function. To test this hypothesis, I generated two *ttna* mutant alleles, *ttna*$^{\Delta 6}$ and *ttna*$^{\Delta 9}$, in zebrafish. *ttna*$^{\Delta 6}$ harbors an 18 bp in-frame deletion and *ttna*$^{\Delta 9}$ has a 27 bp in-frame deletion (Fig. **5B**), which result in 6 and 9 amino acids deletions, respectively. The deleted amino acid sequences of both mutations are in the specific region mentioned above and cover the *TTN* point mutation site (Fig. **5C**).

C. *ttna*$^{\Delta 9/\Delta 9}$ embryos exhibited inflow tract edema and pericardial edema.

Because the deleted regions of *ttna*$^{\Delta 6}$ and *ttna*$^{\Delta 9}$ contain the EOAF-associated *TTN* point mutation site, the zebrafish carrying *ttna*$^{\Delta 6}$ and *ttna*$^{\Delta 9}$ may exhibit an arrhythmia

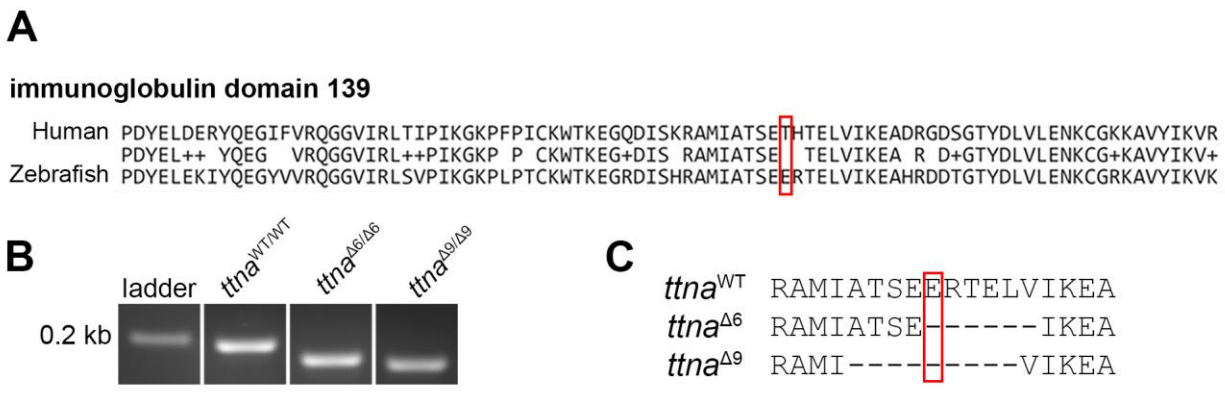

FIGURE 5. *ttna*$^{\Delta 6}$ and *ttna*$^{\Delta 9}$ were generated to reveal the function of the conserved region around the EOAF-associated *TTN* point mutation. (A) Alignment of human Ig-139 domain and its corresponding zebrafish Ig domain. The red box indicates the location of residue affected by the EOAF-associated *TTN* point mutation. **(B)** A 189-bp fragment covering the location of the *TTN* point mutation was amplified, and the electrophoresis revealed an 18-bp deletion in *ttna*$^{\Delta 6/\Delta 6}$, and a 27-bp deletion in *ttna*$^{\Delta 9/\Delta 9}$. **(C)** The amino acid sequences deleted in *ttna*$^{\Delta 6}$ and *ttna*$^{\Delta 9}$ are in the nearby region flanking the EOAF-associated *TTN* point mutation. Sequencing data of allele *ttna*$^{\Delta 6}$ and *ttna*$^{\Delta 9}$ showed the 18-bp deletion and 27-bp deletion result in 6 and 9 amino acids in-frame deletion, respectively. Both in-frame deletions are in the highly conserved region and cover the location affected by the *TTN* point mutation (red box).

phenotype. To test this hypothesis, the heart rhythm of zebrafish carrying *ttna*$^{\Delta 6}$ and *ttna*$^{\Delta 9}$ was assessed using an established method, ZebraPace, which calculates the deviation of heartbeat intervals based on live imaging to determine the heart rhythm(Gaur et al., 2018). Additionally, *ttna* is necessary for sarcomere formation during development, which is important for the normal contraction of cardiomyocytes, so mutations of *ttna* may induce general cardiac defects during development. Therefore, other cardiovascular phenotypes such as edema and blood flow were also assessed in zebrafish embryos carrying *ttna*$^{\Delta 6}$ and *ttna*$^{\Delta 9}$.

While *ttna*$^{\Delta 6/+}$ and *ttna*$^{\Delta 6/\Delta 6}$ embryos showed no difference compared to wild-type embryos, *ttna*$^{\Delta 9/\Delta 9}$ demonstrated multiple cardiac phenotypes. Therefore, the following results focus on *ttna*$^{\Delta 9/\Delta 9}$ embryos.

At 2 dpf, there was no difference in heart rhythm between *ttna*$^{\Delta 9/\Delta 9}$ and wild-type embryos (data not shown). However, 18 out of 19 *ttna*$^{\Delta 9/\Delta 9}$ embryos exhibited inflow tract edema (Fig. **6B**) while 16 out of 17 wild-type embryos and all *ttna*$^{\Delta 9/+}$ embryos did not exhibit edema (Fig. **6A, F**). At 4 dpf, compared to wild-type embryos (Fig. **6C**), all *ttna*$^{\Delta 9/\Delta 9}$ embryos showed pericardial edema at different degrees of severity (Fig. **6G**): mild pericardial edema showed medium swelling in the pericardial area (Fig. **6D**); and severe pericardial edema showed large swelling in the pericardial area (Fig. **6E**). Of note, compared to wild-type embryos (Fig. **6C'**), *ttna*$^{\Delta 9/\Delta 9}$ embryos also showed abnormal atrial shapes with the cardiomyocyte maker cmlc2:eGFP (Huang et al., 2003): 8 out of 10

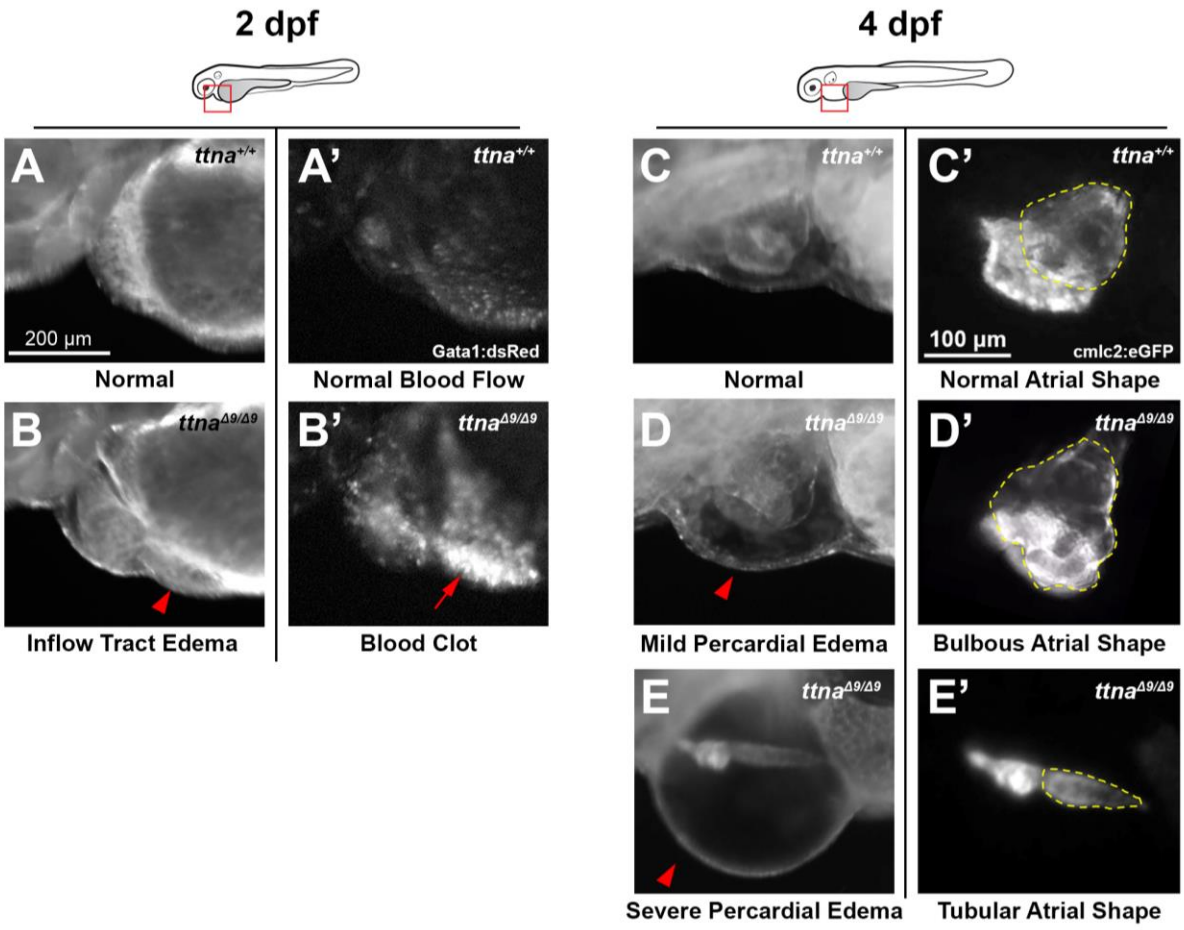
2 dpf
4 dpf
A
ttna+/+
200 µm
Normal
A'
ttna+/+
Gata1:dsRed
Normal Blood Flow
B
ttnaΔ9/Δ9
Inflow Tract Edema
B'
ttnaΔ9/Δ9
Blood Clot
C
ttna+/+
Normal
C'
ttna+/+
100 µm
cmlc2:eGFP
Normal Atrial Shape
D
ttnaΔ9/Δ9
Mild Percardial Edema
D'
ttnaΔ9/Δ9
Bulbous Atrial Shape
E
ttnaΔ9/Δ9
Severe Percardial Edema
E'
ttnaΔ9/Δ9
Tubular Atrial Shape

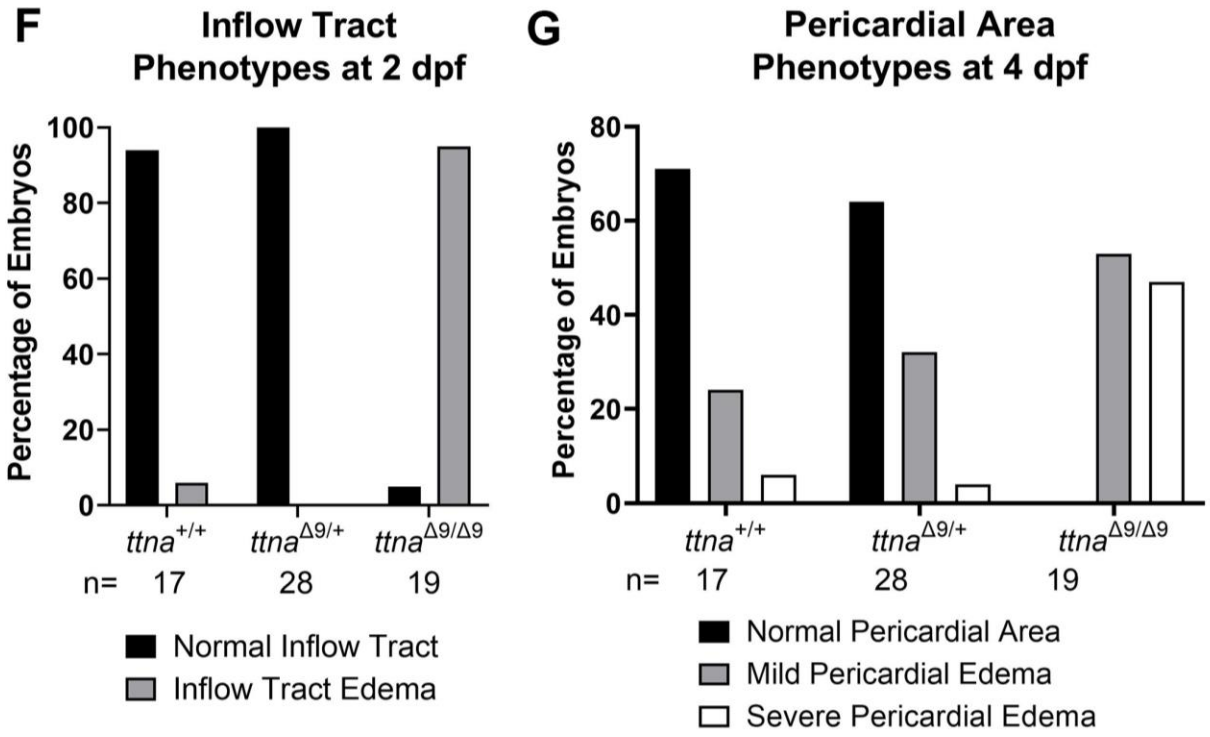
F
Inflow Tract
Phenotypes at 2 dpf
Percentage of Embryos
100
80
60
40
20
0
ttna+/+
ttnaΔ9/+
ttnaΔ9/Δ9
n= 17 28 19
Normal Inflow Tract
Inflow Tract Edema
G
Pericardial Area
Phenotypes at 4 dpf
Percentage of Embryos
80
60
40
20
0
ttna+/+
ttnaΔ9/+
ttnaΔ9/Δ9
n= 17 28 19
Normal Pericardial Area
Mild Pericardial Edema
Severe Pericardial Edema

FIGURE 6. ***ttna*$^{\Delta 9/\Delta 9}$ embryos exhibited inflow tract edema and pericardial edema. (A-B')** At 2 dpf, lateral view of wild-type and *ttna*$^{\Delta 9/\Delta 9}$ zebrafish showing heart area in brightfield **(A, B)** and the blood flow around the heart indicated by red blood cell marker Gata1:dsRed **(A', B')**. **(C-E')** At 4 dpf, lateral view of wild-type and *ttna*$^{\Delta 9/\Delta 9}$ zebrafish showing heart area in brightfield **(C, D, E)** and hearts visualized with cardiomyocyte marker, cmlc2:eGFP, and shapes of atria were indicated by yellow dashed lines **(C', D', E')**. Red arrowheads indicate inflow tract edema and pericardial edema; red arrow indicates blood clot. Locations of heart at 2 and 4 dpf are indicated with red boxes on top. **(F, G)** Quantification of the embryos showing inflow tract edema at 2 dpf and pericardial edema at 4 dpf. Number of embryos in each genotype: *ttna*$^{+/+}$ = 17, *ttna*$^{\Delta 9/+}$ = 28, *ttna*$^{\Delta 9/\Delta 9}$ = 19.

embryos with mild pericardial edema showed a bulbous atrial shape (Fig. **6D'**), and 8 out of 9 embryos with severe pericardial edema showed a tubular atrial shape (Fig. **6E'**) while there was only one wild-type embryo with severe edema showing the tubular atrial shape and no wild-type embryo with mild edema showing bulbous atrial shape. Using the red blood cell marker Gata1:dsRed (Zhu & Zon, 2004), I observed that *ttna*$^{\Delta 9/\Delta 9}$ embryos exhibited blood clot formation in the inflow tract (Fig. **6B'**) and blood regurgitation from the atrium to the inflow tract (data not shown) at 2 dpf, while wild-type embryos showed smooth blood flow and no blood clot (Fig. **6A'**). These data suggest that the *ttna*$^{\Delta 9}$ mutation affects the morphology of atria and induces a weaker circulation that may contribute to fluid accumulation in the inflow tract and pericardial sac.

Currently, genotyping of 3-4 months post-fertilization (mpf) adults from *ttna*$^{\Delta 9/+}$ incrossing and *ttna*$^{\Delta 6/+}$ incrossing show that 7 homozygous mutants can grow to adulthood (**Table II**). The percentage of adult *ttna*$^{\Delta 9/\Delta 9}$ is lower than the 25% expected ratio calculated from Mendelian's law. This result is consistent with embryonic phenotypes that a part of *ttna*$^{\Delta 9/\Delta 9}$ embryos exhibit severe pericardial edema and may not be able to grow to adulthood.

D. *ttna*$^{\Delta 9/\Delta 9}$ embryos had reduced cardiac function.

To understand how the *ttna*$^{\Delta 9}$ mutation affects the circulation, I looked at cardiac contraction at 2 dpf using the transgenic line carrying the cardiomyocyte maker, cmlc2:eGFP (Huang et al., 2003) because inflow tract edema was observed starting from

TABLE II. Genotyping of Adult Zebrafish Carrying *ttna* Mutations

Breeding	Genotypes	Number	Percentage
ttna$^{\Delta 6/+}$ Incrossing	+/+	9	27.3%
	Δ6/+	17	51.5%
	Δ6/Δ6	7	21.2%
ttna$^{\Delta 9/+}$ Incrossing	+/+	13	32.5%
	Δ9/+	20	50%
	Δ9/Δ9	7	17.5%

2 dpf. By measuring the area of atrial lateral view projection at the end of atrial diastole and systole (Fig. **7A**), *ttna*$^{\Delta 9/\Delta 9}$ embryos exhibited larger atrial end-diastolic area and end-systolic area than those of wild-type and *ttna*$^{\Delta 9/+}$ embryos at 2 dpf (Fig. **7B,C)**. The *ttna*$^{\Delta 9/\Delta 9}$ embryos also exhibited a smaller fractional area change (FAC), an indicator for atrial contractility, than did the wild-type embryos (Fig. **7D**). These data indicate that atria of *ttna*$^{\Delta 9/\Delta 9}$ embryos are enlarged and have reduced atrial contractility.

According to the measurement of the area of ventricular lateral view projection, *ttna*$^{\Delta 9/\Delta 9}$ embryos also showed a smaller ventricular FAC (Fig. **7E**). To better assess the function of the heart, I measured the long and short diameters of ventricular lateral view projections (Fig. **7A**) to determine the stroke volume (SV), the blood volume pumped into the body by a single heartbeat, and the ejection fraction (EF), the fraction of ventricular contraction. *ttna*$^{\Delta 9/\Delta 9}$ embryos exhibited decreased SV and EF as compared to the wild-type embryos (Fig. **7F,G**). These results indicate that *ttna*$^{\Delta 9/\Delta 9}$ embryos have reduced cardiac function compared to wild-type embryos. Interestingly, the end-diastolic volume (EDV) of the ventricles of *ttna*$^{\Delta 9/\Delta 9}$ embryos was significantly smaller than that of wild-type and *ttna*$^{\Delta 9/+}$ embryos, but the end-systolic volume (ESV) was not significantly different among the three groups (Fig. **7H,I**). Since SV and EF are calculated from EDV and ESV, these findings suggest a possible defect in ventricular diastole or atrial contraction.

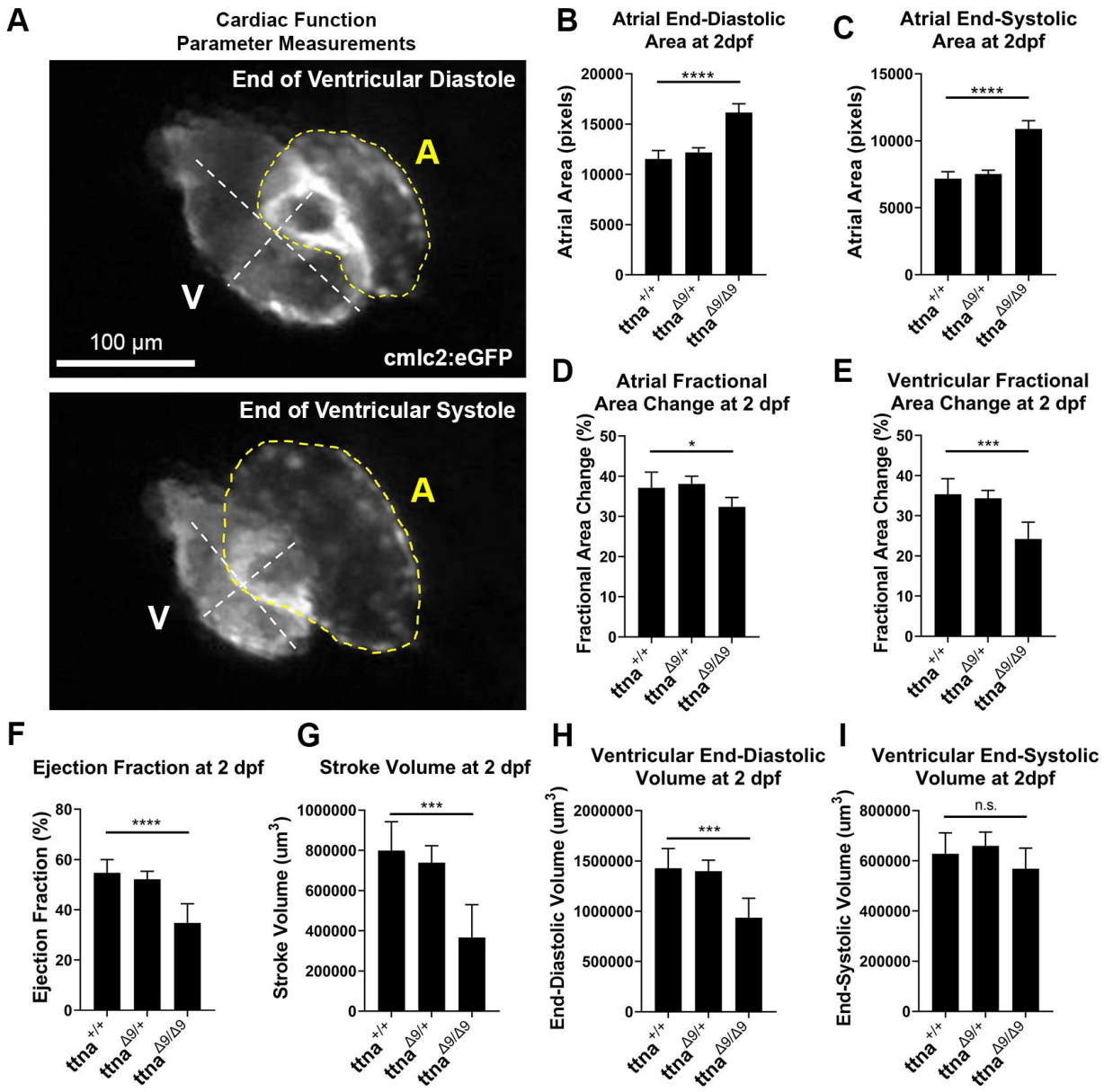

FIGURE 7. ***ttna*$^{\Delta 9/\Delta 9}$ embryos had larger atria and reduced cardiac function at 2 dpf. (A)** Schematic showing the outline of atria used for measuring atrial area (yellow dashed lines) and ventricular short and long diameters (white dashed lines) at the end-diastolic phase and end-systolic phase. **(B, C)** Quantification of the atrial area at the end-diastolic and end-systolic phase. **(D)** Quantification of atrial fractional area change (FAC). **(E-I)** Quantification of ventricular FAC, ejection fraction, stroke volume, ventricular end-diastolic volume and end-systolic volume. Error bars indicate 95% confidence interval. n.s. p>0.05; * p<0.05; *** p<0.001; **** p<0.0001

IV. DISCUSSION

A. A conserved region in a specific Ig domain of ttna is important for proper cardiac function.

In this study, using CRISPR-Cas9 I generated two *ttna* mutant alleles, *ttna*$^{\Delta 6}$ and *ttna*$^{\Delta 9}$. Their deleted regions cover the location of the EOAF-associated *TTN* point mutation and locate in a highly conserved region in a specific Ig domain of ttna. *ttna*$^{\Delta 9/\Delta 9}$ embryos exhibited inflow tract edema and pericardial edema, decreased contraction of atria and ventricles, and decreased cardiac output, while *ttna*$^{\Delta 6/\Delta 6}$ embryos showed no difference from wild-type embryos. These data suggest the deleted region of *ttna*$^{\Delta 9}$ is conserved and important for proper cardiac function.

At 2 dpf, *ttna*$^{\Delta 9/\Delta 9}$ embryos had smaller ventricles than wild-type and *ttna*$^{\Delta 9/+}$ embryos at the end of diastole, but no difference at the end of systole, which resulted in reduced ventricular contraction and cardiac output indicated by lower FAC, SV and EF. Because the only source of blood for the ventricle is the atrium (Gore et al., 2012), so there are two potential explanations for the decreased end-diastolic volume of *ttna*$^{\Delta 9/\Delta 9}$ embryos: 1) the reduced atrial contractility causes a smaller volume of blood to be pumped into the ventricle and results in a smaller ventricle expansion at the end of diastole; 2) a decrease in ventricular cardiomyocyte elasticity makes the ventricle more rigid and harder to expand to accommodate the inflow of blood from the atrium. Since titin is a main component in the sarcomere and necessary for the contraction and relaxation of all

cardiomyocytes (Linke & Hamdani, 2014), the *ttna*$^{\Delta 9}$ mutation may contribute to the phenotype through one or both of the mechanisms above.

AF-related phenotypes including dilated atria and decreased ventricular EF were recapitulated in *ttna*$^{\Delta 9/\Delta 9}$ embryos. The atrial sizes of *ttna*$^{\Delta 9/\Delta 9}$ embryos were larger than those of wild-type and *ttna*$^{\Delta 9/+}$ embryos at the end of diastole and systole. These results suggest that homozygous mutation of *ttna*$^{\Delta 9}$ causes atrial dilation. Dilated atrium has been reported to be associated with AF (Grogan et al., 1992). Additionally, a recent study showed decreases in left ventricular EF presented in mild EOAF patients carrying *TTN* nonsense mutations (Andreasen et al., 2020), which provides a potential association between decreased ventricular EF and EOAF. Therefore, further study of *ttna*$^{\Delta 9}$ phenotypes, such as testing the heart rhythm during adulthood, may provide more evidence and underlying mechanisms for the association between atrial dilation, decreased EF, and EOAF.

B. Further cardiac function assessments for *ttna*$^{\Delta 6}$ and *ttna*$^{\Delta 9}$

To further investigate the potential explanation for the decreased cardiac output, more parameters of cardiac function need to be measured. Besides the current finding of blood clots and regurgitation, more careful measurements of blood velocity and regurgitation at the inflow tract, atrioventricular canal and trunk will provide details of the effects of the *ttna*$^{\Delta 9/\Delta 9}$ deletion on blood circulation. Additionally, a decrease in blood velocity at the atrioventricular canal is one of the symptoms of AF (Goldman et al., 1999),

so investigating blood flow will help determine whether this mutation contributes to an AF-related phenotype other than atrial dilation, decreased EF, and arrhythmia.

Thus far, genotyping of adult zebrafish has identified seven *ttna*$^{\Delta 9/\Delta 9}$ zebrafish that survived the embryonic stage and grew to adulthood. Because embryos with severe pericardial edema had much weaker heart contraction, whole-body edema and usually died around 7 dpf, adult *ttna*$^{\Delta 9/\Delta 9}$ zebrafish likely grew up from embryos that had mild pericardial edema at 4 dpf. These embryos also showed a bulbous atrial shape at 4 dpf. Therefore, more assessments of atria morphology, such as heart dissection and staining, need be done in embryos and adults to reveal details of abnormal atrial shapes caused by *ttna*$^{\Delta 9/\Delta 9}$ mutation. Using these assessments to determine chamber thickening and fibrosis may help us to understand how *ttna*$^{\Delta 9/\Delta 9}$ contributes to abnormal atrial shape phenotypes, why there were different abnormities of atrial shapes, and whether there is an association between these phenotypes and AF because chamber thickening and fibrosis are involved in atrial structural remodeling and AF (Krogh-Madsen et al., 2012; Zuo et al., 2019).

Given that no defect was found in the *ttna*$^{\Delta 9/+}$ embryos and embryos carrying *ttna*$^{\Delta 6}$ and that AF occurs in human adulthood (Morillo et al., 2017), we will conduct additional cardiac functional studies in adult zebrafish carrying these mutant alleles. Determination of cardiac electrophysiology with electrocardiography (ECG) will be done on adult zebrafish to study the heart rhythm and the coordination between the atrium and ventricle

because ECG is a standard diagnostic method for AF and zebrafish have similar ECG characteristics as humans (Orr et al., 2016).

C. Potential mechanisms underlying the phenotypes of *ttna*$^{\Delta 9}$

Titin functions as a scaffold for sarcomere assembly and allows proper contractions of cardiomyocytes (Linke & Hamdani, 2014). Reduced cardiac function of embryos may be caused by defects in the sarcomere assembly during cardiac development. Sarcomere assembly needs to be assessed by visualizing the sarcomere organization with immunofluorescence and electron microscopy. Disorganized sarcomere or loss of specific region(s) of the sarcomere (e.g., M-line and Z-disc) may contribute to the decreased contractility of cardiomyocytes. Additionally, the sarcomere organization of adult zebrafish will be assessed because defective ttna protein may interfere with proper sarcomere organization as the workload of the heart increases. The *ttna*$^{\Delta 9}$ mutation is in the A-band of titin, which is the region for myosin binding (Linke & Hamdani, 2014). It is possible that this mutation affects the binding between titin and myosin, which in turn impacts the sarcomere formation in the cardiomyocytes during zebrafish development and/or sarcomere maintenance in adult zebrafish. Both can lead to a defect in the contractility of the zebrafish heart. Besides testing potential effects of *ttna*$^{\Delta 9}$ deletion on sarcomere organization, electrophysiology characteristics of mutant embryos also need to be tested to explore a potential electrophysiology pathway in the pathology of *ttna*$^{\Delta 9}$, such as a block or delay of ion-channel signal transduction.

The *ttna*$^{\Delta 9}$ mutation may cause degradation of one or more compliant isoforms of titin, resulting in a change in the ratio of compliant to stiff isoforms, thus increasing the diastolic passive stiffness of the heart and decreasing the cardiac output. Recently, an *in vitro* study showed that Ig-139, the Ig domain where *ttna*$^{\Delta 9}$ is located, can interact with MURF1 and direct specific isoform of titin to be degraded through the ubiquitin-proteasome pathway (Higashikuse et al., 2019). This study also found that a hypertrophic cardiomyopathy-associated *TTN* point mutation caused increased degradation of titin, as shown by *in vitro* experiments. Interestingly, this point mutation is in the deleted region of *ttna*$^{\Delta 9}$ but not *ttna*$^{\Delta 6}$, so experiments focusing on titin-MURF1 interaction using *ttna*$^{\Delta 9}$ and *ttna*$^{\Delta 6}$ may help to explain the different phenotypes of embryos carrying *ttna*$^{\Delta 9}$ and *ttna*$^{\Delta 6}$ and reveal a potential mechanism for the current phenotype of *ttna*$^{\Delta 9/\Delta 9}$ embryos.

Titin, as the largest protein discovered in the body spanning half-length of the sarcomere, also has sensing and signaling roles through its binding partners (Linke & Hamdani, 2014). Preliminary observations showed no defect in the organization of skeletal myofibers, and adult *ttna*$^{\Delta 9/\Delta 9}$ zebrafish can swim normally. Given that the affected Ig domain presents in all isoforms of *ttna* in cardiomyocytes and skeletal muscle, heart-specific *TTN*-binding partners or pathways may be involved in the pathology of the *ttna*$^{\Delta 9}$ mutation. Searching for potential downstream targets may give us more insights into this aspect.

A predicted three-dimensional structure of the zebrafish Ig-domain corresponding to the human Ig-139 shows that the deleted regions of *ttna*$^{\Delta 6}$ and *ttna*$^{\Delta 9}$ are in one antiparallel β-sheet (Fig. **8**). The larger deleted region of *ttna*$^{\Delta 9}$ (Fig. **8A**) compared to that of *ttna*$^{\Delta 6}$ (Fig. **8B**) may result in a more severe disruption in the structure of this β-sheet that may be important for the function of this domain, which in turn explains the more severe phenotype of *ttna*$^{\Delta 9}$ compared to that of *ttna*$^{\Delta 6}$. Additionally, the deleted region of *ttna*$^{\Delta 9}$ may even disrupt the structure of the whole domain. To reveal the potential structural disruption caused by *ttna*$^{\Delta 6}$ and *ttna*$^{\Delta 9}$, and to understand the reason for their different phenotypes, more assessments of this domain's structure may be needed in the future.

D. <u>The EOAF-associated *TTN* point mutation study</u>

The generation of the zebrafish line carrying the EOAF-associated *TTN* point mutation will be continued. Even though the current long symmetric HDR template and optimized volume of injection solution have yielded a potential higher efficiency for knocking-in this point mutation, the increased efficiency may still not enough to yield better germline transmission that allows us to generate this zebrafish line in a reasonable period of time.

To further increase the knock-in efficiency, more techniques based on CRISPR-Cas9 can be used as alternatives, including the variation in types of Cas proteins, delivery methods for the ribonucleoprotein complex, and designs of HDR templates. For example,

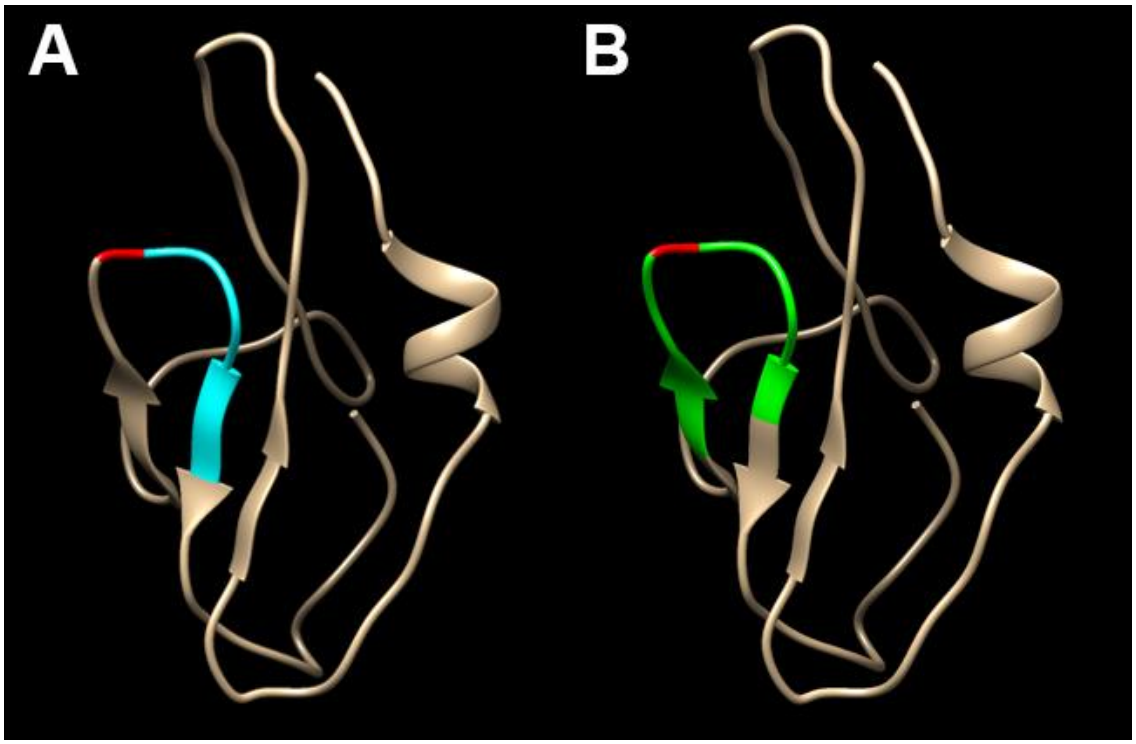

FIGURE 8. Ribbon diagram showing predicted three-dimensional structures of the wild-type zebrafish ttna Ig domain corresponding to the human titin Ig-139 domain. Red regions indicate the residue affected by the EOAF-associated missense point mutation. **(A)** Blue and red regions indicate residues deleted by *ttna*$^{\Delta 6}$. **(B)** Green and red regions indicate residues deleted by *ttna*$^{\Delta 9}$. The three-dimensional structure was predicted by Phyre2 (Kelley et al., 2015).

Cas12a, a type V CRISPR associated protein, has been reported to have higher efficiency for knock-out and knock-in in zebrafish (Moreno-Mateos et al., 2017). More strategies based on microhomology-mediated end joining (Sakuma et al., 2016) and homology-mediated end joining (Yao et al., 2017) have been developed for higher knock-in efficiency. Engineered Cas9 proteins were developed to induce more precise mutation and prevent off-target effects, such as base editor (Zhang et al., 2017) and prime editor (Anzalone et al., 2019). Additionally, chemical treatment with small molecules, such as NHEJ inhibitor (Robert et al., 2015), may increase the knock-in efficiency.

Additionally, because the residue affected by the *TTN* point mutation in human titin is threonine, and the corresponding residue of wild-type zebrafish ttna is glutamate acid, a zebrafish line carrying human wild-type sequence at the location of the *TTN* point mutation will be generated. This line will be tested to determine whether it has the same cardiac development and function as the wild-type zebrafish does, and then can be used as a negative control for the study of the EOAF-associated *TTN* mutation.

In this study, I am using CRISPR-Cas9 to introduce an EOAF-associated *TTN* missense point mutation into the zebrafish to study the underlying mechanism of this mutation in EOAF, and potentially increased the knock-in efficiency by optimizing the method. I also generated two *ttna* mutant alleles, *ttna*$^{\Delta 6}$ and *ttna*$^{\Delta 9}$. Their deleted regions are in the high conserved region flanking the site of the *TTN* point mutation. *ttna*$^{\Delta 9/\Delta 9}$ embryos showed edema and reduced cardiac function, which suggests that the deleted

region of *ttna*$^{\Delta 9}$ is important for proper cardiac function. Further investigating the function of this specific region may reveal more biological pathways that involve titin and contribute to the pathogenesis of EOAF.

CITED LITERATURE

Ahlberg, G., Refsgaard, L., Lundegaard, P. R., Andreasen, L., Ranthe, M. F., Linscheid, N., Nielsen, J. B., Melbye, M., Haunsø, S., Sajadieh, A., Camp, L., Olesen, S.-P., Rasmussen, S., Lundby, A., Ellinor, P. T., Holst, A. G., Svendsen, J. H., & Olesen, M. S. (2018). Rare truncating variants in the sarcomeric protein titin associate with familial and early-onset atrial fibrillation. *Nature Communications, 9*(1). https://doi.org/10.1038/s41467-018-06618-y

Alzahrani, Z., Ornelas-Loredo, A., Darbar, S. D., Farooqui, A., Mol, D., Chalazan, B., Villagrana, N. E., McCauley, M., Lazar, S., Wissner, E., Bhan, A., Konda, S., & Darbar, D. (2018). Association Between Family History and Early-Onset Atrial Fibrillation Across Racial and Ethnic Groups. *JAMA Network Open, 1*(5), e182497-e182497. https://doi.org/10.1001/jamanetworkopen.2018.2497

Andreasen, L., Bertelsen, L., Ghouse, J., Lundegaard, P. R., Ahlberg, G., Refsgaard, L., Rasmussen, T. B., Eiskjær, H., Haunsø, S., Vejlstrup, N., Svendsen, J. H., & Olesen, M. S. (2020, Jun 22). Early-onset atrial fibrillation patients show reduced left ventricular ejection fraction and increased atrial fibrosis. *Sci Rep, 10*(1), 10039. https://doi.org/10.1038/s41598-020-66671-w

Anzalone, A. V., Randolph, P. B., Davis, J. R., Sousa, A. A., Koblan, L. W., Levy, J. M., Chen, P. J., Wilson, C., Newby, G. A., & Raguram, A. (2019). Search-and-replace genome editing without double-strand breaks or donor DNA. *Nature, 576*(7785), 149-157.

Bai, H., Liu, L., An, K., Lu, X., Harrison, M., Zhao, Y., Yan, R., Lu, Z., Li, S., & Lin, S. (2020). CRISPR/Cas9-mediated precise genome modification by a long ssDNA template in zebrafish. *BMC genomics, 21*(1), 1-12.

Banan, M. (2020). Recent advances in CRISPR/Cas9-mediated knock-ins in mammalian cells. *Journal of biotechnology, 308*, 1-9.

Bartos, D. C., Anderson, J. B., Bastiaenen, R., Johnson, J. N., Gollob, M. H., Tester, D. J., Burgess, D. E., Homfray, T., Behr, E. R., Ackerman, M. J., Guicheney, P., & Delisle, B. P. (2013). A KCNQ1 Mutation Causes a High Penetrance for Familial Atrial Fibrillation. *24*(5), 562-569. https://doi.org/10.1111/jce.12068

Brown, D., Samsa, L., Qian, L., & Liu, J. (2016). Advances in the study of heart development and disease using zebrafish. *Journal of cardiovascular*

development and disease, 3(2), 13.

Cazorla, O., Freiburg, A., Helmes, M., Centner, T., McNabb, M., Wu, Y., Trombitas, K., Labeit, S., & Granzier, H. (2000). Differential expression of cardiac titin isoforms and modulation of cellular stiffness. *Circulation Research, 86*(1), 59-67.

Choi, S. H., Weng, L.-C., Roselli, C., Lin, H., Haggerty, C. M., Shoemaker, M. B., Barnard, J., Arking, D. E., Chasman, D. I., Albert, C. M., Chaffin, M., Tucker, N. R., Smith, J. D., Gupta, N., Gabriel, S., Margolin, L., Shea, M. A., Shaffer, C. M., Yoneda, Z. T., Boerwinkle, E., Smith, N. L., Silverman, E. K., Redline, S., Vasan, R. S., Burchard, E. G., Gogarten, S. M., Laurie, C., Blackwell, T. W., Abecasis, G., Carey, D. J., Fornwalt, B. K., Smelser, D. T., Baras, A., Dewey, F. E., Jaquish, C. E., Papanicolaou, G. J., Sotoodehnia, N., Van Wagoner, D. R., Psaty, B. M., Kathiresan, S., Darbar, D., Alonso, A., Heckbert, S. R., Chung, M. K., Roden, D. M., Benjamin, E. J., Murray, M. F., Lunetta, K. L., Lubitz, S. A., & Ellinor, P. T. (2018). Association Between Titin Loss-of-Function Variants and Early-Onset Atrial Fibrillation. *JAMA, 320*(22), 2354. https://doi.org/10.1001/jama.2018.18179

Essner, J. *Zebrafish embryo microinjection Ribonucleoprotein delivery using the Alt-R™ CRISPR-Cas9 System*. https://sfvideo.blob.core.windows.net/sitefinity/docs/default-source/user-submitted-method/crispr-cas9-rnp-delivery-zebrafish-embryos-j-essnerc46b5a1532796e2eaa53ff00001c1b3c.pdf?sfvrsn=52123407_10

Gaur, H., Pullaguri, N., Nema, S., Purushothaman, S., Bhargava, Y., & Bhargava, A. (2018). ZebraPace: an open-source method for cardiac-rhythm estimation in untethered zebrafish larvae. *Zebrafish, 15*(3), 254-262.

Goldman, M. E., Pearce, L. A., Hart, R. G., Zabalgoitia, M., Asinger, R. W., Safford, R., Halperin, J. L., & Investigators, S. P. i. A. F. (1999). Pathophysiologic correlates of thromboembolism in nonvalvular atrial fibrillation: I. Reduced flow velocity in the left atrial appendage (The Stroke Prevention in Atrial Fibrillation [SPAF-III] study). *Journal of the American Society of Echocardiography, 12*(12), 1080-1087.

Gore, A. V., Monzo, K., Cha, Y. R., Pan, W., & Weinstein, B. M. (2012, May). Vascular development in the zebrafish. *Cold Spring Harb Perspect Med, 2*(5), a006684. https://doi.org/10.1101/cshperspect.a006684

Granzier, H., & Labeit, S. (2002). Cardiac titin: an adjustable multi-functional spring. *The Journal of Physiology, 541*(2), 335-342. https://doi.org/10.1113/jphysiol.2001.014381

Grogan, M., Smith, H. C., Gersh, B. J., & Wood, D. L. (1992). Left ventricular dysfunction due to atrial fibrillation in patients initially believed to have idiopathic dilated cardiomyopathy. *The American journal of cardiology, 69*(19), 1570-1573.

Gudbjartsson, D. F., Holm, H., Sulem, P., Masson, G., Oddsson, A., Magnusson, O. T., Saemundsdottir, J., Helgadottir, H. T., Helgason, H., Johannsdottir, H., Gretarsdottir, S., Gudjonsson, S. A., Njølstad, I., Løchen, M.-L., Baum, L., Ma, R. C. W., Sigfusson, G., Kong, A., Thorgeirsson, G., Sverrisson, J. T., Thorsteinsdottir, U., Stefansson, K., & Arnar, D. O. (2017). A frameshift deletion in the sarcomere geneMYL4causes early-onset familial atrial fibrillation. *European Heart Journal, 38*(1), 27-34. https://doi.org/10.1093/eurheartj/ehw379

Herman, D. S., Lam, L., Taylor, M. R. G., Wang, L., Teekakirikul, P., Christodoulou, D., Conner, L., Depalma, S. R., McDonough, B., Sparks, E., Teodorescu, D. L., Cirino, A. L., Banner, N. R., Pennell, D. J., Graw, S., Merlo, M., Di Lenarda, A., Sinagra, G., Bos, J. M., Ackerman, M. J., Mitchell, R. N., Murry, C. E., Lakdawala, N. K., Ho, C. Y., Barton, P. J. R., Cook, S. A., Mestroni, L., Seidman, J. G., & Seidman, C. E. (2012). Truncations of Titin Causing Dilated Cardiomyopathy. *New England Journal of Medicine, 366*(7), 619-628. https://doi.org/10.1056/nejmoa1110186

Higashikuse, Y., Mittal, N., Arimura, T., Yoon, S. H., Oda, M., Enomoto, H., Kaneda, R., Hattori, F., Suzuki, T., Kawakami, A., Gasch, A., Furukawa, T., Labeit, S., Fukuda, K., Kimura, A., & Makino, S. (2019). Perturbation of the titin/MURF1 signaling complex is associated with hypertrophic cardiomyopathy in a fish model and in human patients. *Disease Models & Mechanisms, 12*(11), dmm041103. https://doi.org/10.1242/dmm.041103

Holm, H., Gudbjartsson, D. F., Sulem, P., Masson, G., Helgadottir, H. T., Zanon, C., Magnusson, O. T., Helgason, A., Saemundsdottir, J., Gylfason, A., Stefansdottir, H., Gretarsdottir, S., Matthiasson, S. E., Thorgeirsson, G. M., Jonasdottir, A., Sigurdsson, A., Stefansson, H., Werge, T., Rafnar, T., Kiemeney, L. A., Parvez, B., Muhammad, R., Roden, D. M., Darbar, D., Thorleifsson, G., Walters, G. B., Kong, A., Thorsteinsdottir, U., Arnar, D. O., & Stefansson, K. (2011, Mar 6). A rare variant in MYH6 is associated with high risk of sick sinus syndrome. *Nat Genet, 43*(4), 316-320. https://doi.org/10.1038/ng.781

Howe, K., Clark, M. D., Torroja, C. F., Torrance, J., Berthelot, C., Muffato, M., Collins, J. E., Humphray, S., McLaren, K., Matthews, L., McLaren, S., Sealy, I., Caccamo, M., Churcher, C., Scott, C., Barrett, J. C., Koch, R., Rauch, G.-J., White, S.,

Chow, W., Kilian, B., Quintais, L. T., Guerra-Assunção, J. A., Zhou, Y., Gu, Y., Yen, J., Vogel, J.-H., Eyre, T., Redmond, S., Banerjee, R., Chi, J., Fu, B., Langley, E., Maguire, S. F., Laird, G. K., Lloyd, D., Kenyon, E., Donaldson, S., Sehra, H., Almeida-King, J., Loveland, J., Trevanion, S., Jones, M., Quail, M., Willey, D., Hunt, A., Burton, J., Sims, S., McLay, K., Plumb, B., Davis, J., Clee, C., Oliver, K., Clark, R., Riddle, C., Elliot, D., Threadgold, G., Harden, G., Ware, D., Begum, S., Mortimore, B., Kerry, G., Heath, P., Phillimore, B., Tracey, A., Corby, N., Dunn, M., Johnson, C., Wood, J., Clark, S., Pelan, S., Griffiths, G., Smith, M., Glithero, R., Howden, P., Barker, N., Lloyd, C., Stevens, C., Harley, J., Holt, K., Panagiotidis, G., Lovell, J., Beasley, H., Henderson, C., Gordon, D., Auger, K., Wright, D., Collins, J., Raisen, C., Dyer, L., Leung, K., Robertson, L., Ambridge, K., Leongamornlert, D., McGuire, S., Gilderthorp, R., Griffiths, C., Manthravadi, D., Nichol, S., Barker, G., Whitehead, S., Kay, M., Brown, J., Murnane, C., Gray, E., Humphries, M., Sycamore, N., Barker, D., Saunders, D., Wallis, J., Babbage, A., Hammond, S., Mashreghi-Mohammadi, M., Barr, L., Martin, S., Wray, P., Ellington, A., Matthews, N., Ellwood, M., Woodmansey, R., Clark, G., Cooper, J. D., Tromans, A., Grafham, D., Skuce, C., Pandian, R., Andrews, R., Harrison, E., Kimberley, A., Garnett, J., Fosker, N., Hall, R., Garner, P., Kelly, D., Bird, C., Palmer, S., Gehring, I., Berger, A., Dooley, C. M., Ersan-Ürün, Z., Eser, C., Geiger, H., Geisler, M., Karotki, L., Kirn, A., Konantz, J., Konantz, M., Oberländer, M., Rudolph-Geiger, S., Teucke, M., Lanz, C., Raddatz, G., Osoegawa, K., Zhu, B., Rapp, A., Widaa, S., Langford, C., Yang, F., Schuster, S. C., Carter, N. P., Harrow, J., Ning, Z., Herrero, J., Searle, S. M. J., Enright, A., Geisler, R., Plasterk, R. H. A., Lee, C., Westerfield, M., de Jong, P. J., Zon, L. I., Postlethwait, J. H., Nüsslein-Volhard, C., Hubbard, T. J. P., Roest Crollius, H., Rogers, J., & Stemple, D. L. (2013). The zebrafish reference genome sequence and its relationship to the human genome. *Nature, 496*(7446), 498-503. https://doi.org/10.1038/nature12111

Huang, C.-J., Tu, C.-T., Hsiao, C.-D., Hsieh, F.-J., & Tsai, H.-J. (2003). Germ-line transmission of a myocardium-specific GFP transgene reveals critical regulatory elements in the cardiac myosin light chain 2 promoter of zebrafish. *Developmental Dynamics, 228*(1), 30-40. https://doi.org/10.1002/dvdy.10356

Huttner, I. G., Wang, L. W., Santiago, C. F., Horvat, C., Johnson, R., Cheng, D., von Frieling-Salewsky, M., Hillcoat, K., Bemand, T. J., & Trivedi, G. (2018). A-band titin truncation in zebrafish causes dilated cardiomyopathy and hemodynamic stress intolerance. *Circulation: Genomic and Precision Medicine, 11*(8), e002135.

Kelley, L. A., Mezulis, S., Yates, C. M., Wass, M. N., & Sternberg, M. J. E. (2015, 2015/06/01). The Phyre2 web portal for protein modeling, prediction and

analysis. *Nature protocols, 10*(6), 845-858. https://doi.org/10.1038/nprot.2015.053

Kimmel, C. B., Ballard, W. W., Kimmel, S. R., Ullmann, B., & Schilling, T. F. (1995, Jul). Stages of embryonic development of the zebrafish. *Dev Dyn, 203*(3), 253-310. https://doi.org/10.1002/aja.1002030302

Kotecha, D., & Piccini, J. P. (2015). Atrial fibrillation in heart failure: what should we do? *European Heart Journal, 36*(46), 3250-3257. https://doi.org/10.1093/eurheartj/ehv513

Krogh-Madsen, T., Abbott, G. W., & Christini, D. J. (2012). Effects of electrical and structural remodeling on atrial fibrillation maintenance: a simulation study. *PLoS Comput Biol, 8*(2), e1002390. https://doi.org/10.1371/journal.pcbi.1002390

Lam, P.-Y., & Peterson, R. T. (2019, 2019/06/01/). Developing zebrafish disease models for in vivo small molecule screens. *Current Opinion in Chemical Biology, 50*, 37-44. https://doi.org/https://doi.org/10.1016/j.cbpa.2019.02.005

Letrado, P., de Miguel, I., Lamberto, I., Díez-Martínez, R., & Oyarzabal, J. (2018). Zebrafish: Speeding Up the Cancer Drug Discovery Process. *78*(21), 6048-6058. https://doi.org/10.1158/0008-5472.CAN-18-1029 %J Cancer Research

LeWinter, M. M., & Granzier, H. L. (2013, Feb 26). Titin is a major human disease gene. *Circulation, 127*(8), 938-944. https://doi.org/10.1161/circulationaha.112.139717

Linke, W. A., & Hamdani, N. (2014). Gigantic Business. *Circulation Research, 114*(6), 1052-1068. https://doi.org/10.1161/circresaha.114.301286

Moreno-Mateos, M. A., Fernandez, J. P., Rouet, R., Vejnar, C. E., Lane, M. A., Mis, E., Khokha, M. K., Doudna, J. A., & Giraldez, A. J. (2017). CRISPR-Cpf1 mediates efficient homology-directed repair and temperature-controlled genome editing. *Nature Communications, 8*(1), 1-9.

Morillo, C. A., Banerjee, A., Perel, P., Wood, D., & Jouven, X. (2017). Atrial fibrillation: the current epidemic. *Journal of geriatric cardiology : JGC, 14*(3), 195-203. https://doi.org/10.11909/j.issn.1671-5411.2017.03.011

Orr, N., Arnaout, R., Gula, L. J., Spears, D. A., Leong-Sit, P., Li, Q., Tarhuni, W., Reischauer, S., Chauhan, V. S., Borkovich, M., Uppal, S., Adler, A., Coughlin, S. R., Stainier, D. Y., & Gollob, M. H. (2016, Apr 12). A mutation in the atrial-specific

myosin light chain gene (MYL4) causes familial atrial fibrillation. *Nat Commun, 7*, 11303. https://doi.org/10.1038/ncomms11303

Pinello, L., Canver, M. C., Hoban, M. D., Orkin, S. H., Kohn, D. B., Bauer, D. E., & Yuan, G.-C. (2016). Analyzing CRISPR genome-editing experiments with CRISPResso. *Nature Biotechnology, 34*(7), 695-697. https://doi.org/10.1038/nbt.3583

Poon, K. L., & Brand, T. (2013). The zebrafish model system in cardiovascular research: A tiny fish with mighty prospects. *Glob Cardiol Sci Pract, 2013*(1), 9-28. https://doi.org/10.5339/gcsp.2013.4

Prykhozhij, S. V., Fuller, C., Steele, S. L., Veinotte, C. J., Razaghi, B., Robitaille, J. M., McMaster, C. R., Shlien, A., Malkin, D., & Berman, J. N. (2018). Optimized knock-in of point mutations in zebrafish using CRISPR/Cas9. *Nucleic Acids Research*. https://doi.org/10.1093/nar/gky512

Robert, F., Barbeau, M., Éthier, S., Dostie, J., & Pelletier, J. (2015). Pharmacological inhibition of DNA-PK stimulates Cas9-mediated genome editing. *Genome medicine, 7*(1), 93.

Sakuma, T., Nakade, S., Sakane, Y., Suzuki, K.-I. T., & Yamamoto, T. (2016). MMEJ-assisted gene knock-in using TALENs and CRISPR-Cas9 with the PITCh systems. *Nature protocols, 11*(1), 118-133.

Sarmah, S., & Marrs, J. (2016). Zebrafish as a vertebrate model system to evaluate effects of environmental toxicants on cardiac development and function. *International Journal of Molecular Sciences, 17*(12), 2123.

Seeley, M., Huang, W., Chen, Z., Wolff, W. O., Lin, X., & Xu, X. (2007). Depletion of Zebrafish Titin Reduces Cardiac Contractility by Disrupting the Assembly of Z-Discs and A-Bands. *100*(2), 238-245. https://doi.org/10.1161/01.res.0000255758.69821.b5

Wang, L., Geist, J., Grogan, A., Hu, L.-Y. R., & Kontrogianni-Konstantopoulos, A. (2018). Thick Filament Protein Network, Functions, and Disease Association. *Comprehensive Physiology, 8*(2), 631-709. https://doi.org/10.1002/cphy.c170023

Westerfield, M. (2000). *The zebrafish book. A guide for the laboratory use of zebrafish (Danio rerio)* (4th ed.). Univ. of Oregon Press.

Wilkinson, R. N., Jopling, C., & van Eeden, F. J. (2014). Zebrafish as a model of cardiac

disease. *Prog Mol Biol Transl Sci, 124*, 65-91. https://doi.org/10.1016/B978-0-12-386930-2.00004-5

Yalcin, H. C., Amindari, A., Butcher, J. T., Althani, A., & Yacoub, M. (2017, Nov). Heart function and hemodynamic analysis for zebrafish embryos. *Dev Dyn, 246*(11), 868-880. https://doi.org/10.1002/dvdy.24497

Yamada, N., Asano, Y., Fujita, M., Yamazaki, S., Inanobe, A., Matsuura, N., Kobayashi, H., Ohno, S., Ebana, Y., Tsukamoto, O., Ishino, S., Takuwa, A., Kioka, H., Yamashita, T., Hashimoto, N., Zankov Dimitar, P., Shimizu, A., Asakura, M., Asanuma, H., Kato, H., Nishida, Y., Miyashita, Y., Shinomiya, H., Naiki, N., Hayashi, K., Makiyama, T., Ogita, H., Miura, K., Ueshima, H., Komuro, I., Yamagishi, M., Horie, M., Kawakami, K., Furukawa, T., Koizumi, A., Kurachi, Y., Sakata, Y., Minamino, T., Kitakaze, M., & Takashima, S. (2019, 2019/04/30). Mutant KCNJ3 and KCNJ5 Potassium Channels as Novel Molecular Targets in Bradyarrhythmias and Atrial Fibrillation. *Circulation, 139*(18), 2157-2169. https://doi.org/10.1161/CIRCULATIONAHA.118.036761

Yang, Y., Li, J., Lin, X., Yang, Y., Hong, K., Wang, L., Liu, J., Li, L., Yan, D., Liang, D., Xiao, J., Jin, H., Wu, J., Zhang, Y., & Chen, Y.-H. (2009). Novel KCNA5 loss-of-function mutations responsible for atrial fibrillation. *54*(5), 277-283. https://doi.org/10.1038/jhg.2009.26

Yao, X., Wang, X., Hu, X., Liu, Z., Liu, J., Zhou, H., Shen, X., Wei, Y., Huang, Z., & Ying, W. (2017). Homology-mediated end joining-based targeted integration using CRISPR/Cas9. *Cell research, 27*(6), 801-814.

Zhang, Y., Qin, W., Lu, X., Xu, J., Huang, H., Bai, H., Li, S., & Lin, S. (2017). Programmable base editing of zebrafish genome using a modified CRISPR-Cas9 system. *Nature Communications, 8*(1), 1-5.

Zhu, H., & Zon, L. I. (2004). Use of the DsRed Fluorescent Reporter in Zebrafish. In *Methods in Cell Biology* (Vol. 76, pp. 3-12). Academic Press. https://doi.org/https://doi.org/10.1016/S0091-679X(04)76001-X

Zuo, K., Li, K., Liu, M., Li, J., Liu, X., Liu, X., Zhong, J., & Yang, X. (2019, Apr). Correlation of left atrial wall thickness and atrial remodeling in atrial fibrillation: Study based on low-dose-ibutilide-facilitated catheter ablation. *Medicine (Baltimore), 98*(15), e15170. https://doi.org/10.1097/md.0000000000015170